How to Cite: Kuzieva, M.M., Urishova, F.M., Atakhanov, A.A., Ashurov, N.Sh., Rashidova, S.Sh., Shiman, D.I., Kostjuk, S.V. & Kang, S. (2025). Potassium Permanganate–Oxidized Nanocellulose: Structural Features and Rheological Performance for Advanced Applications. *Eurasian Journal of Chemistry, 30, 4(120), 148–159.* https://doi.org/10.31489/2959-0663/4-25-18

Article

Received: 29 September 2025 | Revised: 26 November 2025 | Accepted: 2 December 2025 | Published online: 9 December 2025

UDC 677.464.1

https://doi.org/10.31489/2959-0663/4-25-18

Makhliyo M. Kuzieva[1], Fayruza M. Urishova[1], Abdumutolib A. Atakhanov[1*], Nurbek Sh. Ashurov[1], Sayyora Sh. Rashidova[1], Dmitriy I. Shiman[2], Sergei V. Kostjuk[3], Saewon Kang[4]

[1]*Institute of Polymer Chemistry and Physics, Tashkent, Uzbekistan;*
[2]*Research Institute for Physical Chemical Problems of the Belarusian State University, Minsk, Belarus;*
[3]*Sorbonne Universite, CNRS, Institut Parisien de Chimie Moleculaire, Sorbonne, France;*
[4]*Korea Research Institute of Chemical Technology, Daejeon, South Korea*
*(*Corresponding author's e-mail: a-atakhanov@yandex.com)*

Potassium Permanganate–Oxidized Nanocellulose: Structural Features and Rheological Performance for Advanced Applications

The development of environmentally friendly strategies for nanocellulose modification is crucial for advancing biomedical materials. Traditional oxidation methods often involve costly or toxic reagents, limiting large-scale use. This study addresses this by preparing oxidized nanocellulose (ONC) from microcrystalline cellulose using an eco-friendly acidic potassium permanganate ($KMnO_4$) oxidation method to introduce surface carboxyl groups. Structural and morphological changes were characterized through FTIR, XRD, SEM, and DLS analyses, which confirmed successful oxidation, retained fibrillar morphology, and altered crystallinity and surface charge. Hydrogel formulations were developed from ONC suspensions, and their rheological properties were assessed through frequency and amplitude sweeps. FTIR spectra confirmed the introduction of carboxyl groups, while XRD revealed reduced crystallinity and lattice expansion with oxidation. DLS demonstrated narrower size distributions at intermediate oxidation times, indicating improved dispersion stability. SEM images confirmed retention of fibrous morphology with reduced fibril widths. Rheological tests showed that ONC hydrogels exhibited shear-thinning and gel-like behavior ($G' > G''$), displaying the highest storage modulus and broadest linear viscoelastic region, consistent with a strong and stable gel network. ONC-based hydrogels show significant promise for biomedical applications, including mucoadhesive drug delivery, wound healing, and tissue engineering.

Keywords: oxidized nanocellulose, microcrystalline cellulose, permanganate oxidation, carboxyl functionalization, structural characterization, hydrogel, rheological properties, drug delivery systems

Introduction

Cellulose, the most abundant biopolymer on Earth, has attracted considerable attention in recent years due to its renewable origin, biodegradability, and versatility in designing advanced functional materials [1]. Chemical modification of cellulose, particularly microcrystalline cellulose (MCC), offers powerful opportunities to tailor its physicochemical properties and expand its applications in biomedicine, drug delivery, and environmental technologies [2, 3]. Among various modification strategies, oxidation is especially important because it introduces functional groups such as carboxyl and aldehyde, thereby enhancing the reactivity, dispersibility, and binding capacity of cellulose derivatives [4, 5].

Conventional oxidants, including 2,2,6,6-tetramethylpiperidine-1-oxyl (TEMPO) [6], sodium periodate ($NaIO_4$) [7], potassium dichromate [8], and ammonium persulfate (APS) [9], have been widely employed to prepare carboxylated and dialdehyde nanocellulose. Despite their effectiveness, these methods often involve expensive reagents and environmentally unfriendly processes.

Consequently, attention has shifted toward greener oxidation routes to obtain oxidized nanocellulose (ONC), which has shown great promise for tissue engineering, wound healing [10], mucoadhesive drug delivery [11, 12], and biosensing applications [13]. The structural and functional properties of ONC are highly dependent on the oxidation pathway, and different oxidizing systems have been explored to tailor these features [14].

In this context, potassium permanganate ($KMnO_4$) in acidic conditions represents a strong yet relatively eco-friendly oxidizing agent. It selectively oxidazes the C6-hydroxyl group of anhydroglucose units, generating carboxyl and carbonyl functionalities [15]. This method is attractive because it is cost-effective, simple to

perform, and produces less toxic by-products compared to chromium-based oxidations [16]. $KMnO_4$ oxidation has been reported to yield surface-functionalized cellulose with improved dispersibility and higher negative surface charge, properties that are crucial for electrostatic interactions in biomedical formulations.

Furthermore, ONC produced by $KMnO_4$ oxidation has been evaluated for its rheological behavior, which is essential for designing injectable hydrogels, thickeners, and bioinks for 3D printing. The entanglement of nanofibrils or nanocrystals governs the flow properties, typically resulting in shear-thinning and viscoelastic responses depending on the oxidation degree and concentration [17, 18]. However, while TEMPO- or periodate-based methods have been extensively studied, the use of acidic $KMnO_4$ oxidation remains underexplored for producing ONC with controlled rheological and structural characteristics [19–21].

Although $KMnO_4$ oxidation of cellulose has been reported previously, studies at the nanoscale level remain scarce. The present findings highlight the significance of acidic $KMnO_4$ oxidation as a cost-effective and environmentally benign pathway for introducing functional groups into nanocellulose. This strategy opens promising opportunities for designing functional cellulose-based materials with tailored structural and rheological properties, particularly in the fields of biomedicine, environmental remediation, and advanced industrial applications.

Therefore, the aim of this work was to synthesize oxidized nanocellulose via acidic potassium permanganate oxidation and to investigate its structural features and rheological properties.

Experimental

Chemicals and Materials

This study used MCC (DP = 240, CrI = 72 %) was produced from cotton cellulose according to the protocol described previously [22]. Potassium permanganate ($KMnO_4$, 99.5 wt%) and sulfuric acid (H_2SO_4, 98.0 wt%) were purchased from Sigma-Aldrich Chemical Co. Ltd. (Tianjin, China). Hydrogen peroxide (H_2O_2) and sodium hydroxide (NaOH, 98.0 %) were obtained from Daejung Chemicals (South Korea). All reagents were of analytical grade and used without further purification. Deionized water was employed throughout all experiments unless otherwise stated.

Preparation of Oxidized Nanocellulose (ONC)

ONC was synthesised in an aqueous medium using potassium permanganate under acidic conditions, following a published method with slight modifications [8]. In a three-neck flask, 3.0 g MCC was dispersed in 50 mL of deionized water and sonicated for 20 min. The suspension pH was adjusted to 2.0 with sulphuric acid, after which 2.34 g $KMnO_4$ was added under continuous magnetic stirring at 50 °C in a glycerin bath. The reaction was carried out for 2 h (sample ONC-2), 3 h (sample ONC-3) and 4 h (sample ONC-4) under nitrogen bubbling. After completion, the reaction was quenched with hydrogen peroxide. The product was centrifuged (8000 rpm, 15 min) and repeatedly washed with deionized water until the pH reached 5. The ONC suspension was then dialyzed against 4.5 L deionised water with 6 water changes over 72 h. The final product was freeze-dried using HetoPowerDry LL3000 Freeze Dryer (Thermo Scientific, UK).

Preparation of ONC-Based Hydrogels

Hydrogels were prepared from oxidized nanocellulose formulations (ONC-2, ONC-3, ONC-4). A 2 % NaOH solution (30 mL) was placed in a three-neck flask covered with aluminum foil, and 3 g ONC was added. The mixture was kept under controlled thawing for 4 h. The samples were subsequently subjected to repeated freeze–thaw cycles until gelation occurred. The resulting gels were washed with distilled water, centrifuged four times (10 min each), and stored at 4 °C prior to use.

Characterization Methods

FTIR

The FTIR spectrometer "Inventio-S" (Bruker) was used and FTIR spectra were recorded in 400–4000 cm^{-1} wavenumber range with a resolution of 2 cm^{-1} and 32 scans at a temperature of 25 °C. All samples were finely ground, dried at 60 °C for 12 h, and pressed into KBr pellets (1 wt%) before analysis. Software of OPUS was applied to determine the peaks at specific points.

Ultraviolet (UV) Spectroscopy

UV spectra of samples were recorded with a Specord 210 UV-spectrophotometer (Analytic Jena, Germany) by using quartz cells 1 cm in diameter and 1 nm slit; the scanning range of measurement was 190–

1000 nm, a scanning speed was 5 nm/s. The aqueous ONC suspensions (0.05 wt%) were ultrasonically dispersed for 15 min prior to measurement.

Atomic force microscopy (AFM)

Morphological studies of ONC were performed by using AFM Agilent 5500 (Agilent, USA). The silicon cantilevers with a stiffness of 9.5 N/m^2 were used and the frequency was 262 kHz. The AFM scan area (x – y – z) was 3.0 – 3.0 – 1 μm.

Wide-Angle X-ray diffraction

XRD studies were carried out using XRD Miniflex 600 (Rigaku, Japan) with monochromatic CuKα radiation isolated by a nickel filter with a wavelength of 1.5418 Å at 40 kV and the current strength of 15 mA. The spectrum was recorded in the interval 2θ = 5°–40°. The air-dried ONC powders were gently ground, mounted on zero-background glass slides, and analyzed under identical sample thickness and humidity conditions. The data processing of experimental diffraction patterns, peak deconvolution, describing the peaks used by Miller indices, peak shape, and the basis for the amorphous contribution were conducted using the software "SmartLab Studio II" and data base PDF-2 (2020 Powder diffraction file, ICDD).

Scanning Electron Microscopy (SEM)

Scanning electron microscopy studies were performed using SEM equipment Veritas-3100 (Korea). Magnification of the device ×10–300000, voltage 200–300 V, maximum scanning area (x÷y÷z) is 120÷120÷65 μm. ONC powder samples obtained by freeze-drying were mounted on double-sided conductive carbon tape and subsequently coated with a thin carbon layer (15–20 nm) using a vacuum sputter coater. SEM images were obtained at an accelerating voltage of 10 kV and a working distance of 10.6 mm.

Dynamic Light Scattering (DLS)

Particle size distribution was measured on a Photocor Compact (Photocor, Russia) at 298 K, using a 635.6 nm semiconductor laser (25 mW). The ONC suspensions were prepared at 0.01 wt%, sonicated for 10 min to disperse aggregates, and filtered through a 0.45 μm PTFE membrane before measurement at 25 °C.

Determination of Carboxyl Group Content

The content of carboxyl groups (mmol/g) was determined by conductometric titration on a Mettler Toledo conductometer (Switzerland). 50 mg ONC was dispersed in 20 mL of 0.01M HCl solution for 15 minutes by using magnetic stirring. Then, the suspension was titrated with a 0.01 M NaOH solution. The number of carboxyl groups was calculated using an equation [23] and expressed in mmol/g. Each batch was titrated three times.

Rheological Measurements

Rheological tests of the hydrogels were carried out using a rotational Rheometer MCR-92 (AntonPaar) equipped with a "cone-plane" type measuring unit (25 mm diameter / 2° angle) at a temperature of 25 °C, shear rate of 0.1–4400 s^{-1}, with 20 s exposure at each step.

Statistical Analysis

All experimental data were collected in triplicates and data expressed as average ± standard deviation. Data were compared using a one-way ANOVA with post-Bonferroni test using GraphPad Prism 5.04 (GraphPad Software Inc.)

Results and Discussion

The ONCs were successfully obtained through acidic potassium permanganate oxidation combined with mild mechanical treatment. The reaction pathway suggests that MnO_4^- ions are initially reduced to Mn^{2+} via oxidation of the C6–OH groups of cellulose. Excess MnO_4^- is subsequently reduced to colloidal MnO_2, which acts as a self-catalyst, thereby enhancing the oxidative capacity of the system (Fig. 1).

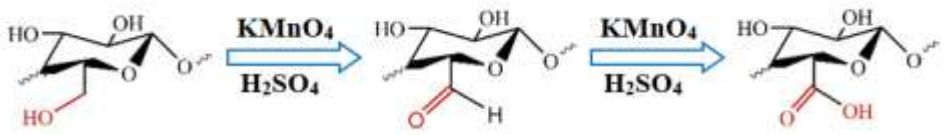

Figure 1. Schematic representation of ONC preparation via potassium permanganate oxidation

Upon completion, the reaction was quenched with hydrogen peroxide, which reduced MnO_2 back to colorless Mn^{2+}. At this stage, the suspension of cellulose nanostructures rapidly turned white, indicating the end of oxidation. The Mn^{2+} ions were efficiently removed during the repeated washing steps. A comparable carboxylation mechanism has been described for oxidation of cellulose nanofibrils [24]. The oxidation of MCC under these conditions proceeds heterogeneously, with the supramolecular organization of cellulose strongly influencing the reaction course [8]. In particular, the C6–OH groups were selectively converted into C6–COOH functionalities, involving electron transfer, proton abstraction, and dehydration steps. This transformation substantially modifies the surface chemistry, charge density, and dispersibility of nanocellulose.

Conductometric titration confirmed that the oxidized samples contained 1.11 mmol/g of carboxyl groups. The successful introduction of these functionalities was further verified by FTIR spectroscopy (Fig. 2).

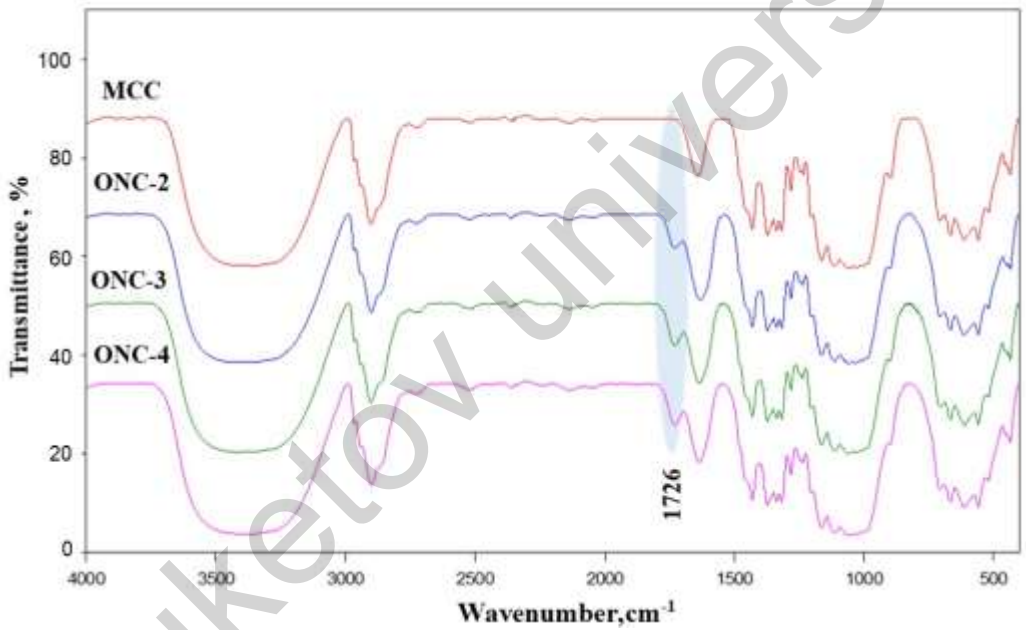

Figure 2. FTIR spectra of MCC, ONC-2, ONC-3 and ONC-4

Comparison of MCC and ONC spectra revealed a broad absorption band near 3415 cm^{-1}, attributed to O–H stretching vibrations. In ONC, this band became sharper and more intense, reflecting a decrease in the number of hydroxyl groups engaged in hydrogen bonding. Stretching vibrations of C–H bonds from methylene and methine groups were detected in the 2800–2900 cm^{-1} region, while a band at 1632 cm^{-1} corresponded to absorbed water, which cannot be fully removed due to strong cellulose–water interactions.

Additional peaks at 1430 cm^{-1}, 1335–1375 cm^{-1}, 1202 cm^{-1}, and 1075–1113 cm^{-1} were assigned to bending vibrations of –CH–, $–CH_2–$, –OH, and –CO groups, together with stretching vibrations of C–O bonds and pyranose rings. Importantly, a new and distinct absorption band at 1726 cm^{-1} was observed in the ONC spectrum, corresponding to C=O stretching vibrations of carboxyl groups, confirming that the primary hydroxyls at the C6 position were oxidized into carboxyl functionalities [25].

The intensity of the C=O band increased with oxidation time: ONC-4 displayed a stronger peak compared to ONC-2, indicating a higher degree of oxidation. Concurrently, the 1425 cm^{-1} band ($–CH_2–$ bending) decreased, while the 1372 cm^{-1} band (out-of-plane $–CH_2–$ vibrations) became more pronounced. These spectral changes suggest a reduction in crystallinity, which was further corroborated by XRD analysis (Fig. 4).

Nevertheless, the persistence of characteristic pyranose ring vibrations confirms that the cellulose backbone remained intact, and oxidation occurred predominantly at the C6 hydroxyl position.

UV–Vis spectroscopic analysis (Fig. 3) revealed characteristic absorption bands for ONC in the 196–202 nm region, associated with electronic transitions of carbonyl-containing groups (aldehydes and carboxyls). A weak shoulder near 230 nm is attributed specifically to C=O transitions of aldehyde functionalities.

The spectra of ONC-2 displayed significantly lower absorbance compared to ONC-3 and ONC-4 across the investigated wavelength range, indicating a lower degree of oxidation and incomplete nanofibrillation. In contrast, ONC-3 and ONC-4 exhibited nearly overlapping spectra with the highest absorbance intensities, consistent with a greater oxidation extent, higher surface charge density, and enhanced colloidal stability. The stronger short-wavelength absorbance in these samples also suggests finer dispersion and reduced particle size, due to increased light scattering in the colloidal state.

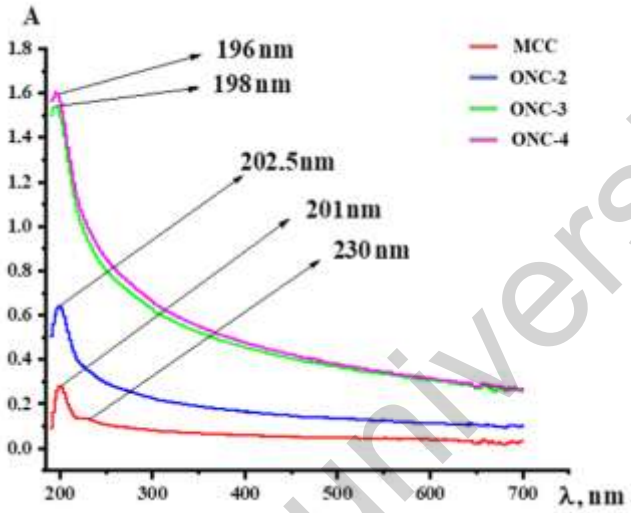

Figure 3. UV spectra of MCC, ONC-2, ONC-3 and ONC-4

For comparison, MCC showed the weakest absorption response, as expected, owing to the absence of UV-active carbonyl groups and the tendency to form larger aggregates, which exhibit limited Rayleigh scattering and lower overall absorbance.

X-ray diffraction (XRD) analysis was performed to evaluate the effect of potassium permanganate oxidation on the crystallinity of MCC (Fig. 4). The diffractograms of MCC and oxidized nanocellulose samples (ONC-2, ONC-3, ONC-4) all exhibited the characteristic reflections of cellulose Iβ, with prominent peaks at $2\theta \approx 14–16°$ (1–10, 110), 22–23° (200), and 34–35° (004). The preservation of these reflections indicates that the native cellulose I lattice was retained after oxidation, consistent with previous reports on TEMPO- and periodate-oxidized cellulose nanostructures [26].

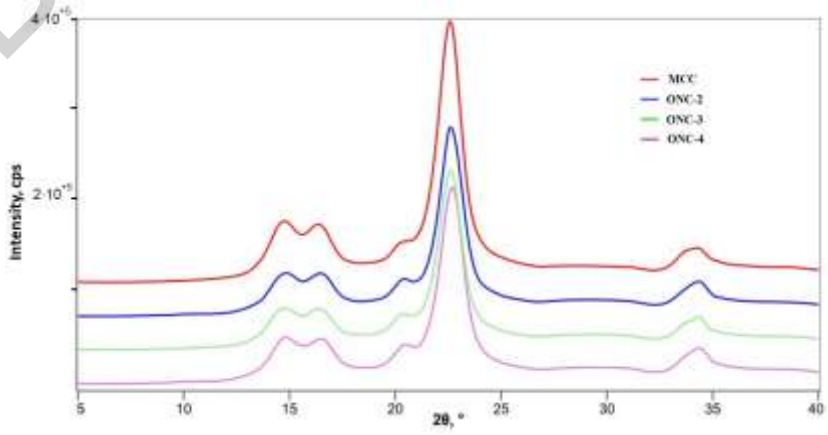

Figure 4. X-ray diffraction patterns of MCC, ONC-2, ONC-3 and ONC-4

MCC displayed the most intense and sharp (200) reflection, indicative of a high degree of crystalline order. With increasing oxidation time, the intensity of the crystalline peaks decreased progressively (ONC-2>ONC-3>ONC-4) and reflections became broader, confirming a gradual reduction in crystallinity and disruption of long-range order. This loss of crystallinity is attributed to the incorporation of carboxyl and aldehyde groups, which disturb inter- and intramolecular hydrogen bonding within the native lattice [27].

The (200) reflection shifted slightly toward lower 2θ values with increasing oxidation time. Calculated d-spacings expanded from ~3.90 Å (MCC) to ~4.00 Å (ONC-4), suggesting that bulky, hydrophilic groups introduced at the C6 hydroxyl (and partially at C2/C3) increase the intersheet separation along the a-axis of the monoclinic unit cell. This expansion is consistent with electrostatic repulsion and hydration effects previously reported in carboxylated cellulose nanofibers [28].

Analysis of the full width at half maximum (FWHM) of the (200) peak revealed progressive broadening, corresponding to reduced crystallite dimensions. Scherrer analysis showed a decrease in crystallite size from ~7–8 nm (MCC) to ~4 nm (ONC-4), consistent with fragmentation of crystalline domains**.** Such reduction reflects enhanced lattice disorder and partial depolymerization, phenomena also observed in TEMPO-oxidized cellulose fibrils [29].

Overall, the data indicate that oxidation produces two concurrent structural effects: (i) expansion of the cellulose lattice**,** due to functional group substitution and hydration, and (ii) reduction of crystallite size, due to chain scission and disorder. At higher oxidation levels (ONC-4), these effects accumulate, yielding a material with predominantly amorphous character and only residual crystalline order.

Importantly, the progressive decline in crystallinity correlates with the rheological performance of ONC-based hydrogels. MCC, although highly crystalline, exhibited weak gel strength due to poor interparticle interactions. ONC-3, with moderate crystallinity and sufficient functionalization, provided the best balance between structural order and surface activity, resulting in optimal network interactions and enhanced mechanical resilience. In contrast, ONC-4 showed extensive lattice disruption, consistent with its reduced storage modulus and premature yielding. These findings highlight that an intermediate oxidation state (ONC-3) achieves the most favorable structural balance for hydrogel performance.

Dynamic light scattering (DLS) analysis revealed clear differences in the particle size distribution of MCC and ONC samples as a function of oxidation time (Fig. 5). Native MCC exhibited a broad and polydisperse profile, with a main population in the 100–500 nm range and a secondary fraction extending into the micron scale. This heterogeneity reflects the tendency of MCC to agglomerate due to limited dispersibility.

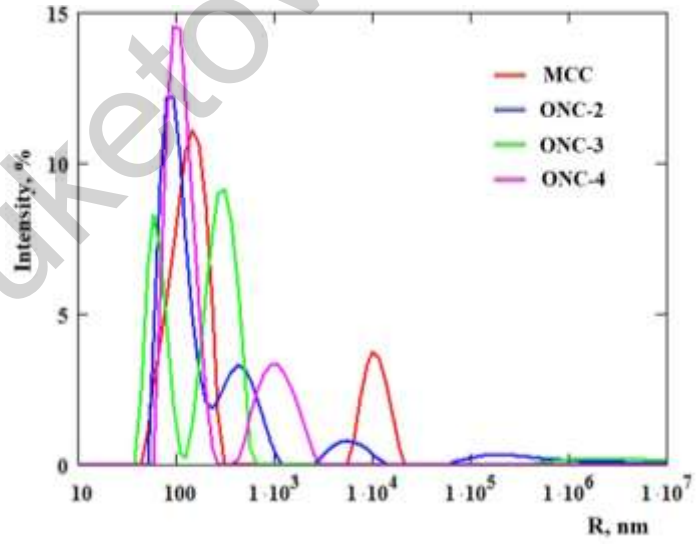

Figure 5. DLS size distributions of MCC, ONC–2, ONC-3 and ONC–4

Oxidation induced a pronounced shift toward smaller and narrower particle size distributions, confirming that the introduction of carboxyl groups enhanced electrostatic stabilization. ONC-2 showed two populations: a dominant peak near ~200 nm and a minor fraction above 1 μm, indicating partial fibril disintegration with residual aggregates. ONC-3 displayed the sharpest and most intense peak at 100–150 nm, with minimal larger fractions, signifying efficient oxidation, high colloidal stability, and uniform dispersion.

In contrast, ONC-4 exhibited a bimodal distribution with a primary peak near 100 nm and a secondary fraction above 500 nm. This suggests that prolonged oxidation induced partial re-aggregation, likely due to excessive chain scission and weakening of the fibrillar framework, which compromised steric stabilization. Such behavior is consistent with FTIR and XRD data, where ONC-4 showed pronounced lattice disruption and higher densities of oxidized groups.

These results underscore the close link between oxidation degree and colloidal stability. Moderate oxidation **(**ONC-3**)** produced the most homogeneous nanoparticle distribution, while insufficient oxidation **(**ONC-2**)** left aggregates intact and over-oxidation **(**ONC-4**)** introduced heterogeneity through structural degradation. These trends align with previous reports on oxidized nanocellulose dispersions, where carboxylation improves stability up to an optimal level, beyond which colloidal uniformity decreases [28].

It should be noted that the dynamic light scattering (DLS) technique has certain limitations when applied to anisotropic nanocellulose systems. As emphasized by Filippov et al. [30], the DLS method assumes that particles are spherical and isotropic scatterers. In the case of fibrillar materials such as ONS, this assumption may lead to an overestimation of the hydrodynamic diameter and an inaccurate interpretation of the size distribution. Moreover, the presence of polydisperse populations, inter-fibrillar interactions, and orientation effects can significantly influence the intensity-weighted size values obtained by DLS. Therefore, the DLS data in this study should be interpreted as providing a relative measure of colloidal dispersion quality rather than an absolute representation of particle dimensions.

The morphological characteristics of ONC were investigated by SEM, which provided detailed visualization of particle shape, size distribution, and surface structure. Due to their high surface energy, ONC particles exhibited a marked tendency to agglomerate, forming clusters at both the nano- and microscale.

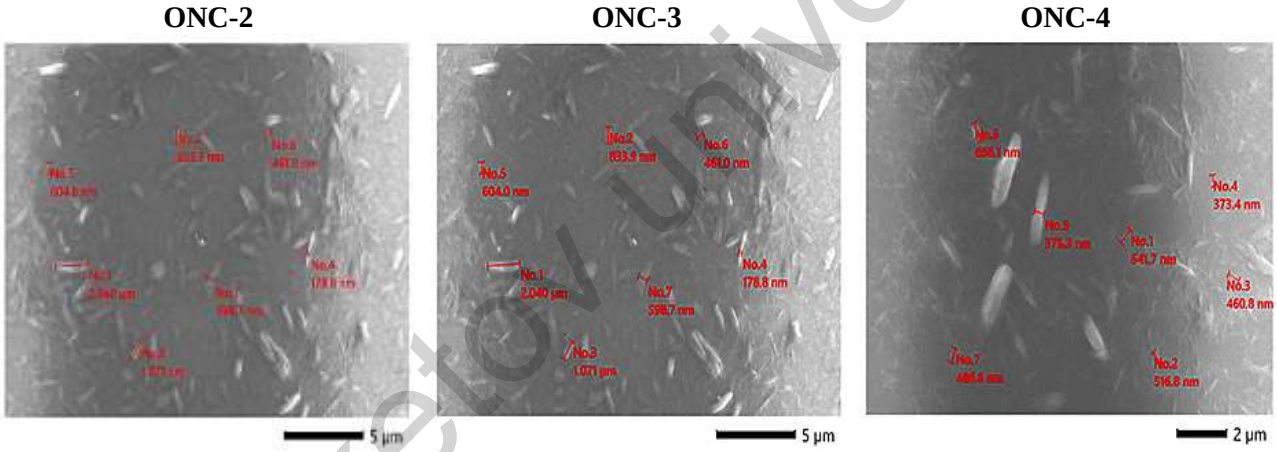

Figure 6. SEM images of ONC-2, ONC-3 and ONC-4

SEM analysis demonstrated a clear relationship between oxidation time and particle dimensions. With prolonged reaction duration, the average width of ONC fibrils progressively decreased from ~12–20 nm to ~3–5 nm, while maintaining a fibrous morphology. The fibril lengths were in the range of 200–500 nm (Fig. 6). Extended oxidation led to the formation of finer and more uniform nanofibers, resulting in a more homogeneous nanoscale network.

The successful fabrication of hydrogels and cryogels from ONC highlights its versatility as a functional biopolymer for biomedical applications. As illustrated in Figure 7, ONC was dissolved in an alkaline medium (2 % NaOH)**,** followed by controlled freezing and freeze-drying, yielding three-dimensional porous cryogels. This behavior parallels earlier findings on TEMPO-oxidized cellulose, which also forms robust and morphologically controlled hydrogels and films [27].

The freezing-induced ice-templating process generated a distinctive porous architecture, ideal for water uptake, solute diffusion and etc. The introduction of carboxyl and carbonyl groups in ONC enhanced solubility. Hydrogen bonding plays a central role in stabilization: intermolecular bonds contribute elasticity and resilience, while intramolecular bonds ensure structural integrity. This dual mechanism yields scaffolds with high porosity, and tunable swelling capacity. SEM image confirmed a sponge-like porous network (Fig. 7), consistent with previous reports on nanocellulose-based aerogels and hydrogels [31].

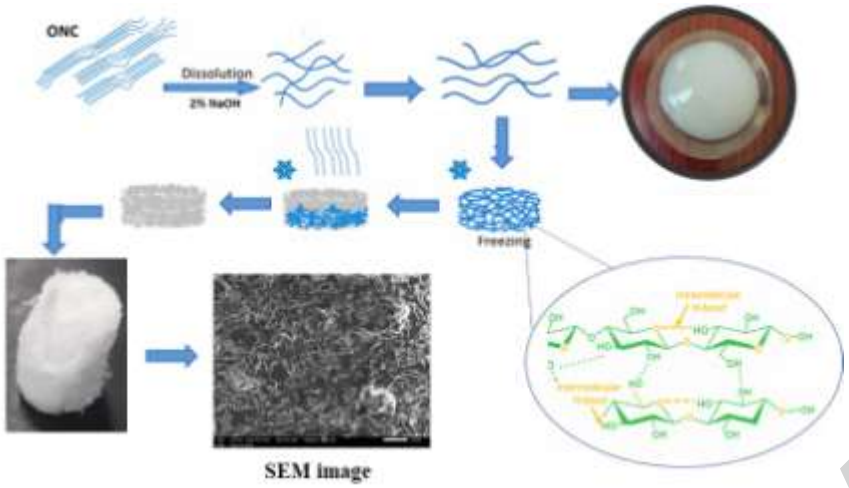

Figure 7. Schematic illustration of the preparation of ONC-based hydrogels and cryogels

Importantly, these ONC-based hydrogels were fabricated without synthetic crosslinkers, providing an eco-friendly and inherently biocompatible route to advanced biomaterials [32].

Rheological characterization provides essential insights into the mechanical integrity and stability of hydrogels [33]. Both frequency sweep and amplitude sweep experiments were conducted to evaluate the viscoelastic performance of ONC hydrogels. These tests allow differentiation between solid-like and liquid-like behaviour, determination of the linear viscoelastic region (LVE), and identification of the yield point**,** where the internal network collapses (Fig. 8).

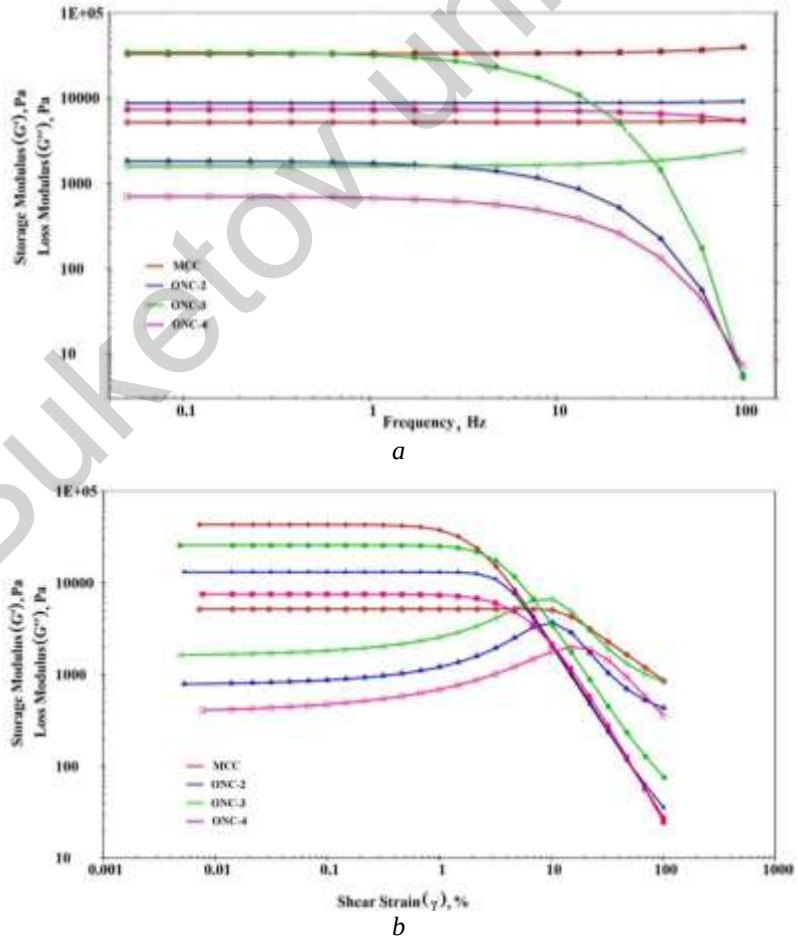

Figure 8. Frequency- (*a*) and amplitude- (*b*) sweep curves of ONC hydrogels

In frequency sweeps, a stable gel is defined by a frequency-independent storage modulus (G′) dominating over the loss modulus (G″). All ONC hydrogels exhibited G′ > G″ throughout the frequency range, confirming their predominantly elastic character. In contrast, MCC showed a relatively high damping factor (tan δ ≈ 0.9), consistent with weak elasticity and viscous predominance. Oxidation markedly enhanced network strength: ONC-2 displayed improved elasticity, while ONC-3h achieved the highest G′ values (10^4–10^5 Pa) and the lowest tan δ (~0.1–0.2), characteristic of a strong, stable gel network stabilized by carboxyl groups. ONC-4, however, exhibited declining G′ at higher frequencies, indicative of network fatigue and partial breakdown caused by cellulose chain scission during prolonged oxidation.

Amplitude sweeps further clarified the strain-dependent stability of gels. Within the LVE, both G′ and G″ remained constant, reflecting intact networks; beyond this region, G′ decreased and eventually crossed G″ at the yield point. MCC hydrogels displayed a narrow LVE and early yielding **(**γ ≈ 15–20 %**)**, highlighting poor resistance to deformation. ONC-2 extended the LVE slightly (~20–25 %), whereas ONC-3 showed the broadest LVE (~25–30 %) and the highest G′ plateau, exemplifying a "true gel" with excellent stability under deformation and strong cohesive forces. ONC-4 again yielded earlier (~15–20 %) with reduced moduli, confirming the detrimental effects of excessive oxidation.

Taken together, both rheological tests demonstrate that ONC-3 hydrogels strike the optimal balance between functionalization and structural integrity. They combine frequency-independent elasticity, a broad LVE, and high yield strain — hallmarks of robust gel networks. In contrast, ONC-2 and ONC-4 deviate from this profile due to insufficient and excessive oxidation, respectively. These findings are highly relevant for the design of nanocellulose-based hydrogels tailored to biomedical applications such as mucoadhesion, drug delivery, and wound healing**.**

Conclusions

In this study, microcrystalline cellulose was successfully oxidized with potassium permanganate to produce oxidized nanocellulose with tunable structural and functional properties. Systematic characterization revealed that the oxidation time critically governed crystallinity, surface chemistry, particle size distribution, and rheological performance of the resulting materials.

FTIR analysis confirmed the introduction of carboxyl groups at the C6 hydroxyl position, while XRD indicated progressive loss of crystallinity, lattice expansion, and crystallite size reduction with increasing oxidation. DLS measurements showed enhanced colloidal stability and narrower size distributions at intermediate oxidation, whereas prolonged treatment led to partial re-aggregation. Rheological studies identified ONC-3 hydrogels as the strongest and most stable, displaying high storage modulus, a broad linear viscoelastic region, and superior deformation resistance compared with under- or over-oxidized samples.

Taken together, the results demonstrate that intermediate oxidation (3 h) offers the optimal balance between functionalization and structural preservation, yielding nanocellulose with enhanced dispersion stability, crystallinity, and mechanical robustness. This work advances the understanding of structure–property relationships in oxidized nanocellulose and identifies ONC-3 as a promising platform for biomedical hydrogels, particularly in mucoadhesive drug delivery, wound healing, and tissue engineering.

Funding

This research was supported by the Basic Fundamental Program of the Academy of Sciences of the Republic of Uzbekistan, and the Uzbekistan–Belarus joint project funded by the Ministry of Higher Education, Science and Innovation of the Republic of Uzbekistan (Grant No. FL-8824063315, X25UZB-126).

*Author Information**

**The authors' names are presented in the following order: First Name, Middle Name and Last Name*

Makhliyo Mukhammadievna Kuzieva — PhD, Junior Researcher, Institute of Polymer Chemistry and Physics, Abdulla Kadiri street, 7-b, 100128, Tashkent, Uzbekistan; e-mail: makhliyokuziyeva92@gmail.com; https://orcid.org/0000-0003-2552-6941

Fayruza Murod qizi Urishova — Junior Researcher, Institute of Polymer Chemistry and Physics, Abdulla Kadiri street, 7-b, 100128, Tashkent, Uzbekistan; e-mail: urishovafayruza600@gmail.com; https://orcid.org/0009-0001-8798-9522

Abdumutolib Abdupatto o'g'li Atakhanov (*corresponding author*) — Doctor of Technical Sciences, Professor, Director of Institute of Polymer Chemistry and Physics, Abdulla Kadiri street, 7-b, 100128, Tashkent, Uzbekistan; e-mail: a-atakhanov@yandex.com; https://orcid.org/0000-0002-4975-3658

Nurbek Shodievich Ashurov — Candidate of Physical and Mathematical Sciences, Senior Researcher, Institute of Polymer Chemistry and Physics, Abdulla Kadiri street, 7-b, 100128, Tashkent, Uzbekistan; e-mail: ansss72@mail.ru; https://orcid.org/0000-0001-5246-434X

Sayyora Sharafovna Rashidova — Doctor of Science, Professor, Academician, Consultant of Director, Institute of Polymer Chemistry and Physics, Abdulla Kadiri street, 7-b, 100128, Tashkent, Uzbekistan; e-mail: polymer@academy.uz; https://orcid.org/0000-0003-1667-4619

Dmitriy Ivanovich Shiman — Senior Researcher, Research Institute for Physical Chemical Problems of the Belarusian State University, Leningradskaya str., 14, 220006, Minsk, Belarus; e-mail: ShimanD@bsu.by; https://orcid.org/0000-0001-8810-9825

Sergei Viktorovich Kostjuk — Research Director, Sorbonne Universite, CNRS, Institut Parisien de Chimie Moleculaire, 4 Pl. Jussieu, 75005, Paris, France; e-mail: Kostjuks@bsu.by, sergei.kostjuk@sprbonne-universite.fr; https://orcid.org/0000-0002-7466-3662

Saewon Kang — Professor, Korea Research Institute of Chemical Technology, 141 Gajeong-ro, Yuseong District, 34114, Daejeon, South Korea; e-mail: skang@krict.re.kr; https://orcid.org/0000-0001-5932-6636

Author Contributions

The manuscript was written through contributions of all authors. All authors have given approval to the final version of the manuscript. CRediT: **Kuzieva Makhliyo Mukhammadievna** investigation, validation, writing-original draft; **Urishova Fayruza Murod qizi** investigation, methodology, formal analysis; **Abdumutolib Abdupatto o'g'li Atakhanov** conceptualization, data curation, formal analysis, validation, writing-review & editing; **Nurbek Shodievich Ashurov** conceptualization, data curation, investigation, methodology, visualization, writing-original draft, writing-review & editing; **Sayyora Sharafovna Rashidova** conceptualization, supervision, editing; **Dmitriy Ivanovich Shiman** formal analysis, editing; **Sergei Viktorovich Kostjuk** formal analysis, editing; **Saewon Kang** formal analysis, editing.

Declaration of Generative AI and AI-Assisted Technologies in the Writing Process

During the preparation of this work the authors used Grammarly in order to refine the language of the manuscript. After using this service, the authors reviewed and edited the content as needed and take full responsibility for the content of the publication.

Conflicts of Interest

The authors declare no conflict of interest.

References

1 Seddiqi, H., Oliaei, E., Honarkar, H., Jin, J., Geonzon, L. C., Bacabac, R. G., & Klein-Nulend, J. (2021). Cellulose and its derivatives: towards biomedical applications. *Cellulose*, *28*(4), 1893–1931. https://doi.org/10.1007/s10570-020-03674-w

2 Lupidi, G., Pastore, G., Marcantoni, E., & Gabrielli, S. (2023). Recent developments in chemical derivatization of microcrystalline cellulose (mcc): pre-treatments, functionalization, and applications. *Molecules*, *28*(5), 2009. https://doi.org/10.3390/molecules28052009

3 Shakhabutdinov, S.Sh., Yugay, S.M., Ashurov, N.Sh., Ergashev, D.J., Atakhanov, A.A., & Rashidova, S.Sh. (2024). Characterization electrospun nanofibers based on cellulose triacetate synthesized from licorice root cellulose. *Eurasian Journal of Chemistry*, 2(114), 21–31. https://doi.org/10.31489/2959-0663/2-24-2

4 Aziz, T., Farid, A., Haq, F., Kiran, M., Ullah, A., Zhang, K., Li, C., Ghazanfar, S., Sun, H., Ullah, R., Ali, A., Muzammal, M., Shah, M., Akhtar, N., Selim, S., Hagagy, N., Samy, M., & Al Jaouni, S. K. (2022). A review on the modification of cellulose and its applications. *Polymers*, 14(15), 3206. https://doi.org/10.3390/polym14153206

5 Goyibnazarov, I. S., Yuldoshov, S. A., Sarymsakov, A. A., Yunusov, K. E., Yarmatov, S. S., Shukurov, A. I. & Wan, Y. (2025). Obtaining dialdehyde carboxymethylcellulose through microwave treatment. *Advances in Polymer Technology*, 1, 9917563. https://doi.org/10.1155/adv/9917563

6 Abraham, E., Deepa, B., Pothan, L. A., Jacob, M., Thomas, S., Cvelbar, U., & Anandjiwala, R. (2011). Extraction of nanocellulose fibrils from lignocellulosic fibres: A novel approach. *Carbohydrate Polymers*, *86*(4), 1468–1475. https://doi.org/10.1016/j.carbpol.2011.06.034Get rights and content

7 Choi, H. N., Yang, H. S., Chae, J. H., Choi, T. L., & Lee, I. H. (2020). Synthesis of conjugated rod–coil block copolymers by RuPhos Pd-catalyzed Suzuki–Miyaura catalyst-transfer polycondensation: initiation from coil-type polymers. *Macromolecules*, *53*(13), 5497–5503. https://doi.org/10.1021/acs.macromol.0c00949

8 Kuzieva, M., Atakhanov, A.A., Shahobutdinav, S., Ashurov, N.S., Yunusov, K.E., & Guohua, J (2023). Preparation of oxidized nanocellulose by using potassium dichromate. *Cellulose*, *30*, 5657–5668. https://doi.org/10.1007/s10570-023-05222-8

9 Saba, F., Mohammad, H.N., Navid, R., & Siavash, I (2023). *ACS Biomaterials Science & Engineering*, 9(6), 2949–2969 https://doi.org/10.1021/acsbiomaterials.3c00300

10 Bayer, I.S. (2021). A review of sustained drug release studies from nanofiber hydrogels. *Biomedicines*, *9*(11), 1612. https://doi.org/10.3390/biomedicines9111612

11 Atakhanov, A.A., Ashurov, N.Sh., Kuzieva, M.M., Mamadiyorov, B.N., Ergashev, D.J., Rashidova, S.S., & Khutoryanskiy, V.V. (2024). Novel acryloylated and methacryloylated nanocellulose derivatives with improved mucoadhesive properties. *Macromolecular Bioscience*, 2400183 (1–10). https://doi.org/10.1002/mabi.202400183

12 Balcerak-Woźniak, A., Dzwonkowska-Zarzycka, M., & Kabatc-Borcz, J. (2024). A Comprehensive Review of Stimuli-Responsive Smart Polymer Materials — Recent Advances and Future Perspectives. *Materials*, *17*(17), 4255. https://doi.org/10.3390/ma17174255

13 Tortorella, S., Vetri Buratti, V., Maturi, M., Sambri, L., Comes Franchini, M., & Locatelli, E. (2020). Surface-modified nanocellulose for application in biomedical engineering and nanomedicine: A review. *International journal of nanomedicine*, 9909–9937. https://doi.org/10.2147/IJN.S266103

14 Mehwish, H. M., Liu, G., Rajoka, M. S. R., Cai, H., Zhong, J., Song, X., & He, Z. (2021). Therapeutic potential of Moringa oleifera seed polysaccharide embedded silver nanoparticles in wound healing. *International Journal of Biological Macromolecules*, 184, 144–158. https://doi.org/10.1016/j.ijbiomac.2024.138116

15 Hassan, R. M., & Ibrahim, S. M. (2024). Review on synthesis of novel carbonyl derivatives of biological macromolecules by oxidation of polysaccharides with permanganate ion in alkaline media. *Journal of Umm Al-Qura University for Applied Sciences*, *10*(2), 348–366. https://doi.org/10.1007/s43994-023-00098-7

16 Guan, X., He, D., Ma, J., & Chen, G. (2010). Application of permanganate in the oxidation of micropollutants: a mini review. *Frontiers of Environmental Science & Engineering in China*, *4*(4), 405–413. https://doi.org/10.1007/s11783-010-0252-8

17 Zhou, S., Han, C., Ni, Z., Yang, C., Ni, Y., & Lv, Y. (2022). Gelatin-oxidized nanocellulose hydrogels suitable for extrusion-based 3D bioprinting. *Processes*, *10*(11), 2216. https://www.mdpi.com/2227-9717/10/11/2216

18 Won, T., Goh, M., Lim, C., Moon, J., Lee, K., Park, J., & Gwon, K. (2025). Recent Progress in Cellulose Nanofibril Hydrogels for Biomedical Applications. *Polymers*, *17*(17), 2272. https://doi.org/10.3390/polym17172272.

19 Jaffar, S. S., Saallah, S., Misson, M., Siddiquee, S., Roslan, J., Saalah, S., & Lenggoro, W. (2022). Recent development and environmental applications of nanocellulose-based membranes. *Membranes*, *12*(3), 287. https://doi.org/10.3390/membranes12030287

20 Liu, S., Tian, Z., & Ji, X.X. (2024). Preparation and modification of nanocellulose using deep eutectic solvents and their applications. *Cellulose*, 31, 2175–2205. https://doi.org/10.1007/s10570-024-05738-7

21 Rouhi, M., Garavand, F., Heydari, M., Mohammadi, R., Sarlak, Z., Cacciotti, I., & Parandi, E. (2024). Fabrication of novel antimicrobial nanocomposite films based on polyvinyl alcohol, bacterial cellulose nanocrystals, and boric acid for food packaging. *Journal of Food Measurement and Characterization*, *18*(3), 2146–2161. https://doi.org/10.1007/s11694-023-02325-5

22 Atakhanov, A. A., Kholmuminov, A. A., Mamadierov, B. N., Turdikulov, I. Kh., & Ashurov, N. Sh. (2020). Rheological Behavior of Nanocellulose Aqueous Suspensions. *Polym. Sci. Series A*, *62*(3), 213–217. https://doi.org/10.1134/S0965545X20030013

23 Habibi, Y., Chanzy, H., & Vignon, M. R. (2006). TEMPO-mediated surface oxidation of cellulose whiskers. *Cellulose*, *13*(6), 679–687. https://doi.org/10.1007/s10570-006-9075-y

24 Pan, R., Cheng, Y., Pei, Y., Liu, J., Tian, W., Jiang, Y., & Zheng, X. (2023). Cellulose materials with high light transmittance and high haze: a review. *Cellulose*, 30(8), 4813–4826. https://doi.org/10.21203/rs.3.rs-1310113/v1

25 Yusuf, M. O. (2023). Bond characterization in cementitious material binders using Fourier-transform infrared spectroscopy. *Applied Sciences*, *13*(5), 3353.25. https://doi.org/10.3390/app13053353

26 Yang, B., Zhang, M., Lu, Z., Tan, J., Luo, J., Song, S., & Zhang, Q. (2019). Comparative study of aramid nanofiber (ANF) and cellulose nanofiber (CNF). *Carbohydrate polymers*, *208*, 372–381. https://doi.org/10.3390/app13053353

27 Isogai, A., Saito, T., & Fukuzumi, H. (2011). TEMPO-oxidized cellulose nanofibers. *Nanoscale*, *3*(1), 71–85. https://doi.org/10.1039/C0NR00583E

28 Saito, T., Nishiyama, Y., Putaux, J. L., Vignon, M., & Isogai, A. (2006). Homogeneous suspensions of individualized microfibrils from TEMPO-catalyzed oxidation of native cellulose. *Biomacromolecules*, 7(6), 1687–1691. https://doi.org/10.1021/bm060154s

29 Alexander, S. P., Mathie, A., Peters, J. A., Veale, E. L., Striessnig, J., Kelly, E., & Zhu, M. (2021). The concise guide to pharmacology 2021/22: Ion channels. *British Journal of Pharmacology*, *178*, S157–S245. https://doi.org/10.1111/bph.15539

30 Filippov S.K., Khusnutdinov R., Murmiliuk A., Inam W., Zakharova L.Ya., Zhang H., & Khutoryanskiy V.V. (2023). Dynamic light scattering and transmission electron microscopy in drug delivery: a roadmap for correct characterization of nanoparticles and interpretation of results. *Materials Horizons*, 10, 5354–5370. https://doi.org/10.1039/D3MH00717K

31 Huo, Y., Liu, Y., Xia, M., Du, H., Lin, Z., Li, B., & Liu, H. (2022). Nanocellulose-Based Composite Materials Used in Drug Delivery Systems. *Polymers*, 14(13), 2648. https://doi.org/10.3390/polym14132648

32 Zhang, H. (2018). *Ice templating and freeze-drying for porous materials and their applications.* John Wiley & Sons. https://doi.org/10.1002/9783527807390.ch10

33 Mezger, T. (2020). *The rheology handbook: for users of rotational and oscillatory rheometers.* European Coatings. https://doi.org/10.1515/arh-2002-0029